Dynamics of chemical reactions of multiply-charged cations: Information from beam scattering experiments

Zdenek Herman *

V. Čermák Laboratory, J. Heyrovský Institute of Physical Chemistry, Academy of Sciences of the Czech Republic, Dolejškova 3, 182 23 Prague 8, Czech Republic

A B S T R A C T

Results of beam scattering experiments on dynamics of chemical (bond-forming) reactions of molecular dications and trications are briefly reviewed. Both studies of crossed-beam scattering experiments and experiments using advanced position-sensitive coincidence method and their achievements that added to a better understanding of collisional mechanisms and energy deposition in products of this class of processes are discussed. In addition, results of other non-scattering methods (mass spectrometric, guided beam, time-of-flight) are briefly mentioned, if relevant to the subject of the paper.

© 2014 Elsevier B.V. All rights reserved.

1. Introduction

For many decades the stage of ion chemistry and physics was dominated by studies of properties and collision processes of singly-charged ions, cations, and to a lesser extent anions. In the past forty years or so, the interest in studies of multiply-charged ions has been growing rapidly. This is evidenced by review articles on properties of multiply-charged ions [1], on the stability of multiply-charged molecular species [2], on their spectroscopy [3,4], and on their gas-phase reactivity [5–8].

Studies of multiply-charged ions as collision species date back to interest of physicists in electron transfer (charge transfer, electron exchange) processes, e.g.,

$$A^{n+} + B \rightarrow A^{(n-1)+} + B^{+} \tag{1}$$

(where A, B are atoms or simple molecules) over a wide range of energies, especially at energies of 100 eV and higher (up to keV). Several reviews provide an overview of the work done [5,8–10]. Rather naturally, the first objective was to study the electron transfer processes of atomic multiply-charged ions with atomic ions. Though the existence of molecular multiply-charged ions has been known since the twenties [11], more detailed information–both experimental and theoretical–on the stability of these species, their electronic structure, spectroscopic properties, energetics, and their behavior in collisions–in particular in electron transfer processes–came in the eighties and nineties. Models have

been developed [1,9,10] to describe electron transfer between an atomic doubly-charged ion and a neutral atomic target, a specific variant of Reaction (1). Transitions between potential terms of the reactants (ion-induced dipole interaction dication–neutral) and the products (Coulomb repulsion between two singly-charged ions), crossing at acute angles, are well localized. The Landau–Zener (L–Z) formalism can be then applied in most cases to describe the transition probability. An important conclusion of this approach is the "reaction window" concept: the electron transfer process proceeds efficiently only if the crossings between the reactant and product potential energy terms fit into a certain range of internuclear separations (qualitatively, for internuclear separations too large, the terms cross diabatically for small separations, they are adiabatically split–in both cases the reactant-product transitions are hindered).

In view of the fact that electron transfer processes have been studied by beam methods (translational energy spectroscopy) mostly at fairly large collision energies, it is not surprising that information on chemical reactions of multiply-charged ions (sometimes referred to as bond-forming reactions), namely reactions of the type

$$A^{2+}BC \rightarrow AB^{+} + C^{+} \tag{2}$$

came from a different type of experiments whose domain were thermal or near-thermal collision energies (flowing afterglows, Fourier transform ion cyclotron resonance – FT ICR). The first experiments concerned atomic metal dications and probably the very first mention of such reactions was contained in a flowing afterglow study of electron transfer processes between Ca^{2+} and Mg^{2+} with simple molecules, indicating the possibility of

* Tel.: +420 266 053 514; fax: +420 286 582 307l.
E-mail address: zdenek.herman@jh-inst.cas.cz (Z. Herman).

formation of $CaO^+ + NO^+$ in reactions of these ions with NO_2 [12]. Formation of NO_2^+ in the reaction of O_2^{2+} with NO was mentioned in a selected-ion drift tube study of rate coefficients of the oxygen dication reactions [13]. An important flowing afterglow study [14,15] of the reactivity of Ti^{2+} with simple alkanes and a comparison with reactivity of the respective singly-charged metal ion described a series of chemical reactions of the metal dication, effectively competing with electron transfer processes. FT ICR studies [16–18] of the reactivity of other metal dications (Nb^{2+}, Ta^{2+}, Zr^{2+}, La^{2+}, Y^{2+}) with C1-C4 alkanes revealed, beside effective electron transfer, formation of protonated metal cations MeH^+ in chemical reactions of the type

$$Me^{2+} + RH \rightarrow MeH^+ + R^+ \tag{3}$$

and also the formation of dication chemical products, e.g. [16]

$$Nb^{2+} + CH_4 \rightarrow NbCH_2^{2+} + H_2 \tag{4}$$

Bond-forming reactions of mixed metal cluster dications (e.g. $LaFe^{2+}$ YFe^{2+}) and alkanes were described, too [16]. Guided-beam and theoretical studies of reactions between Ta^{2+} and methane [19] provided information on bond energies of the species involved, mapped the potential energy surfaces and intermediates and suggested that the products were formed through a $H–Ta^{2+}–CH_3$ intermediate.

However, it was only in 1994 that chemical reactions of non-metal molecular dications as CF^{2+}, CF_2^{2+}, CF_3^{2+}, CO_2^{2+}, or OCS^{2+} [20] with simple molecules (D_2, O_2, N_2, NO, CO) were described. The authors used a crossed-beam arrangement combined with a time-of-flight product detection and described a series of both non-dissociative and dissociative electron transfer and bond-forming reactions of the dications together with the relative abundance of different product ions formed; the results were consistent with the Landau–Zener curve-crossing mechanism. The bond-forming reactions were of two different classes, transfer of a negative ion to the dication or a positive ions transfer to the neutral reactant. This opened a way for detailed studies of the dynamics of reactions of molecular dications in scattering crossed-beam experiments.

This review concentrates largely on results of beam scattering studies of the dynamics of bond-forming reactions of molecular dications and their mechanisms in which both velocity and angle of the product ions were determined. Other beam experiments are discussed only if related to this subject. Electrospray ionization has provided an excellent way to produce multiply-charged metal clusters, liganded and solvated metal clusters [21], biopolymer ions and enabled studies of their properties, dissociations, and reactivity. Also, it enabled studies of multiply-charged (positive or negative) ion–ion (negative or positive) reactions as reviewed elsewhere [22]. However, these results will not be discussed in this article.

2. Experimental methods

A typical low-resolution crossed-beam apparatus used in the early studies of dication electron transfer and bond-forming reactions of, e.g., CF_2^+ [23,24] or CO_2^{2+} [25] with deuterium was the Prague apparatus EVA II (Fig. 1) [23,26]. The dications were produced by impact of 130 eV electrons on a suitable gas (CF_4, CO_2, CH_3Cl) in a low pressure ion source. Ions were extracted, mass analyzed, and decelerated by a multielement lens to the required laboratory energy. The dication beam was crossed at right angles with a beam of molecules of the neutral reagent emerging from a multichannel jet. The ion beam had an angular and energy spread of $1°$ and 0.3 eV (full-width-at half-maximum, FWHM), respectively; the collimated neutral beam had an angular spread of $6°$ (FWHM) and thermal energy distribution at 300 K. Reagent and product ions passed through a detection slit (2.5 cm from the scattering center) into a stopping potential energy analyzer, they were then accelerated and focused into the detection mass spectrometer, mass analyzed, and detected with the use of a dynode electron multiplier. Angular distributions were obtained by rotating the two beams about the scattering center. Modulation of the neutral beam and phase-sensitive detection of the ion products was used to remove the background scattering effects.

Laboratory angular distributions and energy profiles recorded at a series of laboratory scattering angles were used to construct scattering diagrams of the product ions showing contours of the Cartesian probability distribution [26] and normalized to the maximum in the particular scattering diagram. Center-of-mass (CM) angular distributions (relative differential cross sections), $P(\theta_{CM})$ vs. θ_{CM}, and relative translational energy distributions, $P(T')$ vs. T', of the product ions were obtained by appropriate integration of the scattering diagrams [26] (the designation T' is used for
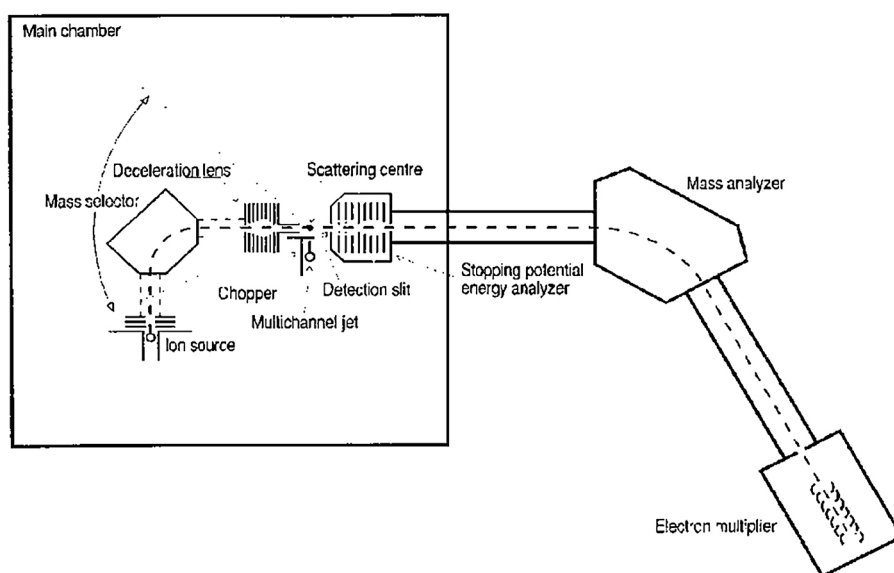

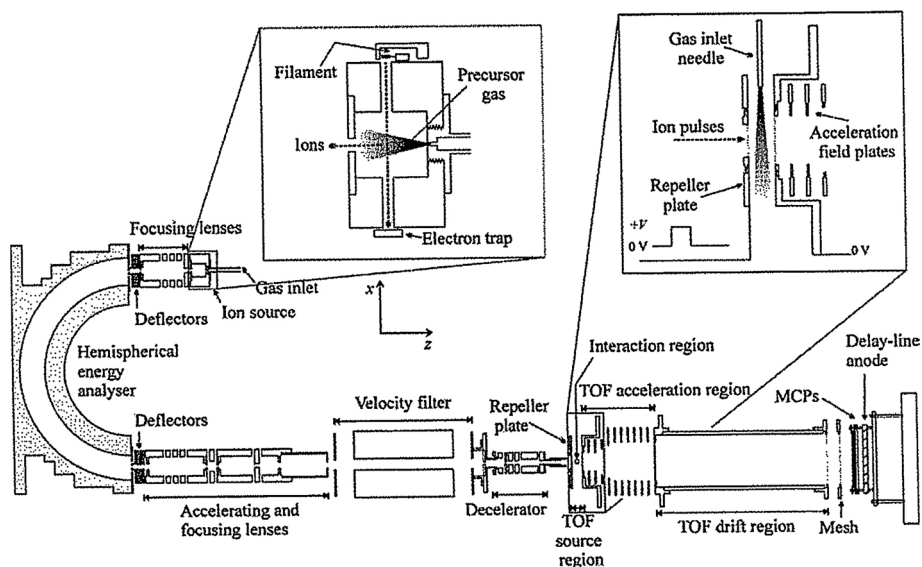**Fig. 1.** Schematics of the crossed-beam apparatus EVA II.

Fig. 2. Schematics of the position-sensitive coincidence apparatus (PSCO). Insets are enlargements of the ion source and the dication–neutral reaction zone localized in the source region of the time-of-flight mass spectrometer.

relative translational energy of products and T for relative translational energy of reagents). A certain limitation of these studies is interpretation of dissociative reactions in which more than two products are formed. Detection of only one product ion requires the assumption that further dissociation of the product ion takes place subsequently to the interaction of the dication–neutral reagents. This assumption appeared to be correct in the systems studied, but coincidence experiments on other systems indicated that this may not be always the case.

The crossed-beam scattering method that has overcome this problem was the position-sensitive coincidence method (PSCO) developed for studies of dication collisions at the University College London, based on the detection of pairs of fragment ions

[27–29]. The apparatus (Fig. 2) produced ions by electron impact ionization from a suitable precursor gas, the ions (singly- and doubly-charged) were extracted from the ion source and passed through a hemispherical analyzer of a good resolution and transmission (final energy spread set to about 0.3 eV). The ion beam was then pulsed across a small aperture and the pulsed packets of ions were formed by a series of focusing and accelerating lenses, passed through a commercial velocity filter to produce dication packets that were decelerated to a desired incident energy of a few eV. They interacted then with the neutral gas emerging from an effusive jet in the source/reaction of the time-of-flight mass spectrometer (TOF-MS). In the source region, originally field-free, a strong voltage pulse was applied to the ion
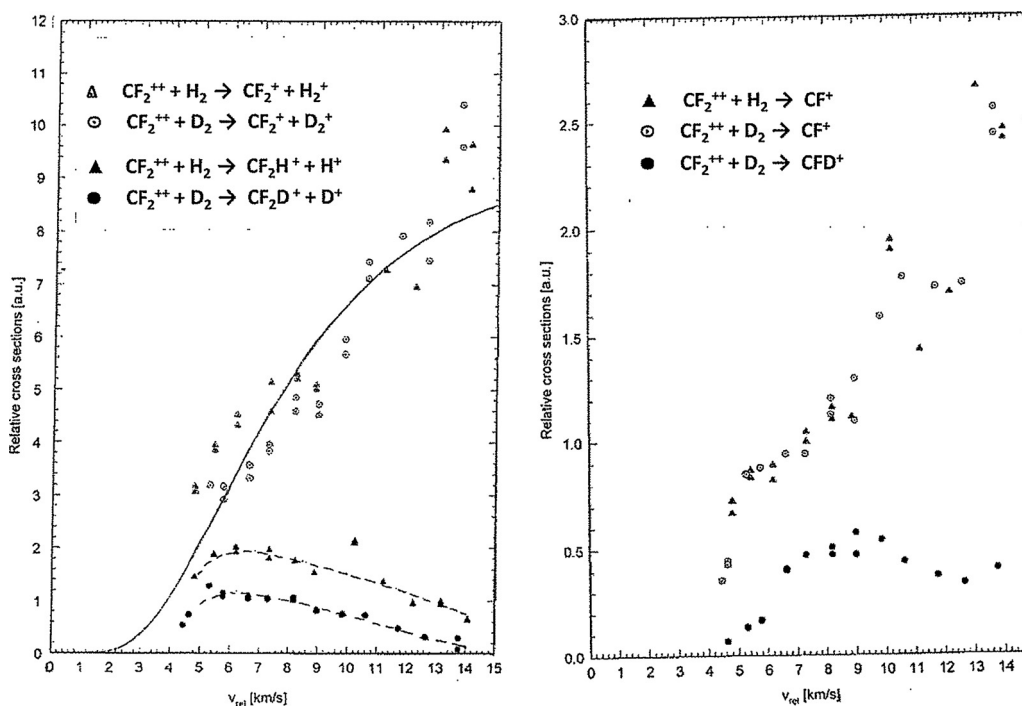

Fig. 3. Relative total cross sections of non-dissociative electron transfer and chemical reactions of CF_2^{2+} with H_2 and D_2 (left) and for the dissociative reactions (right) as a function of the reagent relative velocity v_{rel}. The solid line is the Landau–Zener fit for the electron transfer reaction.
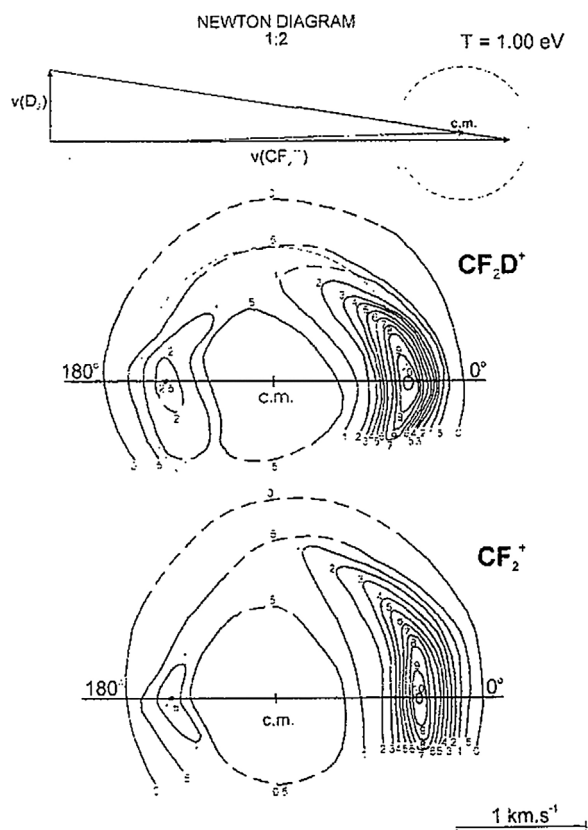
Fig. 4. Contour scattering diagrams of products CF_2D^+ and CF_2^+ from Reactions (6) and (5), respectively, collision energy 1.00 eV. Upper part shows the respective Newton diagram (in a reduced scale 0.5:1), the horizontal line marks the direction of the reagent relative velocity vector.

repeller plate which started the TOF analysis. The arrival times of ions were collected on a pair of multi-channel plates and by emission of electrons from them their position on the position-sensitive detector. The arrival of each ion was then characterized by five times (4 from wires of the position-sensitive system and one from the multi-channel plate). A dataset of 10 times characterizing each pair of ions was available and the data were further processed off-line. The final products were scattering diagrams usually plotted so that the upper and lower halves showed the velocities of

the two ions of the detected pair (see later on). Though the diagrams were somewhat different from the earlier conventional scattering diagrams, the data could be obviously used to obtain the same dynamical quantities. The coincidence experiments have been especially useful in studying the dynamics of dissociative bond-forming reactions and greatly enhanced the possibilities of scattering experiments.

Crossed-beam devices without angular and energy analysis were used in determining total cross sections and branching of products of bond-forming reactions of dications [20,30].

Other beam methods used to study chemical reactions of molecular dications include different mass spectrometric methods [31,32], guided-beam methods [33] or a special apparatus combining selected-ion-flow-tube with the guided ion beam method [31], in combination with isotope labeling and appearance energy measurements of ions.

3. Results

3.1. Crossed beam scattering experiments

3.1.1. $CF_2^{2+} + D_2$: Competition of electron transfer and chemical reactions

The system $CF_2^{2+} + D_2(H_2)$ was the first system studied by scattering in crossed beams [23,24]. Earlier data on the reactions occurring in it [20] showed dominating electron transfer (5) and a bond-forming reaction giving CF_2D^+ (6), besides dissociative processes leading to CF^+ and CFD^+.

$$CF_2^{2+} + D_2 \rightarrow CF_2^+ + D_2^+ \tag{5}$$

$$\rightarrow CF_2D^+ + D^+ \tag{6}$$

Relative total cross sections of all these processes were measured [24]. They are shown in Fig. 3 plotted against the relative velocity of the colliding reagents. The cross section for the dominating electron transfer increased with increasing relative velocity, it was the same for both D_2 and H_2 and its shape was consistent with relations derived from the Landau–Zener formalism. The dissociative process to CF^+ (about 30% of the non-dissociative electron transfer) also increased in a similar way (Fig. 3) and so pointed out to subsequent dissociation of the electron transfer product CF_2^+. The total cross section of the product of the bond-forming Reaction (6) at first slightly increased and then slowly decreased with increasing v_{rel} (Fig. 3). There was a
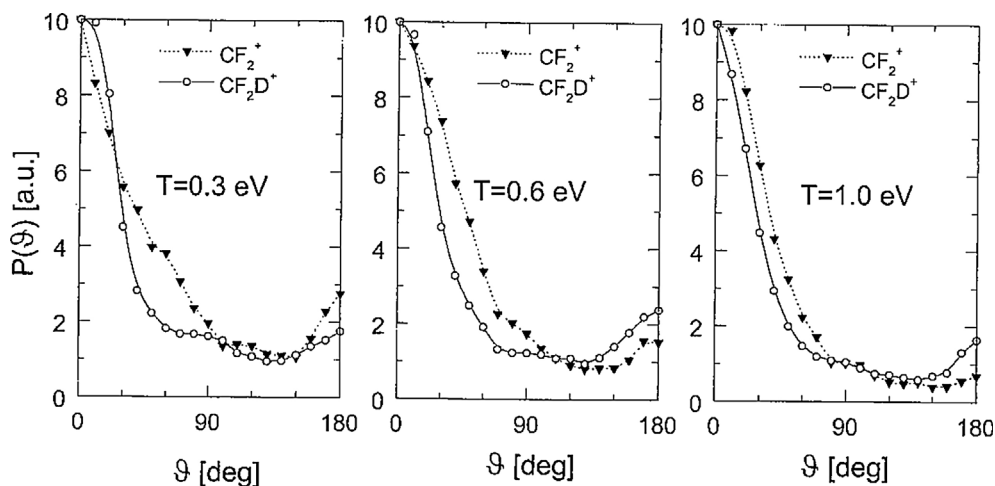

Fig. 5. Relative differential cross sections (CM angular distributions), $P(\vartheta)$ vs. ϑ, of CF_2D^+ (solid line) and CF_2^+ dotted) from Reactions (6) and (5) at the indicated collision energies T.
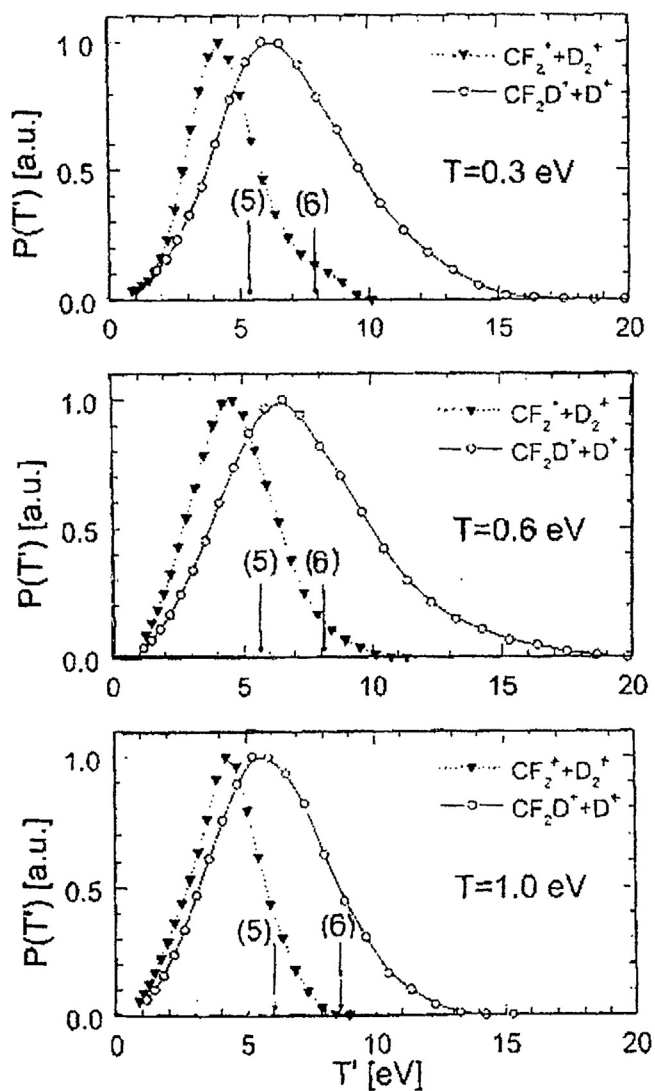
Fig. 6. Relative translational energy distributions, $P(T')$ vs. T', of products from Reactions (5) and (6) at the indicated collision energies T. Arrows mark the maximum energy available in the reactions.

Fig. 7. Schematics of the potential energy model for competition of electron transfer and chemical reactions in dication–molecule collisions showing simplified potential energy surfaces and their possible crossings.

clear isotope effect favoring chemical Reaction (6) with H_2 over D_2 by about 1.5–2. The dissociative product CFD^+ (Fig. 3) evidently originated from further dissociation of CF_2D^+.

Fig. 4 shows the respective scattering diagrams of CF_2D^+ and CF_2^+ at a collision energy of 1.0 eV. The diagrams are superficially similar. The non-dissociative electron transfer (CF_2^+) shows a strongly forward scattered product, as in other electron transfer processes studied before (see, e.g., Ref. [8,34]), reflecting an electron transfer prevailingly at larger internuclear distances with small angular deflection from the original direction of the colliding species. The product of the chemical non-dissociative reaction shows a little more of backward scattering, indicating partly more intimate encounters. This is reflected in the CM angular distributions (relative differential cross sections) in Fig. 5, where the backward scattering in case of the chemical reaction is somewhat stronger (the anomaly at 0.30 eV is probably and experimental inaccuracy). Fig. 6 summarizes the data on relative translational energy distributions of both reaction products, $P(T')$ vs. T'. Due to the inconvenient mass ratio of the products and the small recoil of heavy CF_2^+ and CF_2D^+ on D_2^+ and D^+, respectively, and the resulting spread in the scattering diagrams, the translational energy distribution tail much beyond the limit set by the total
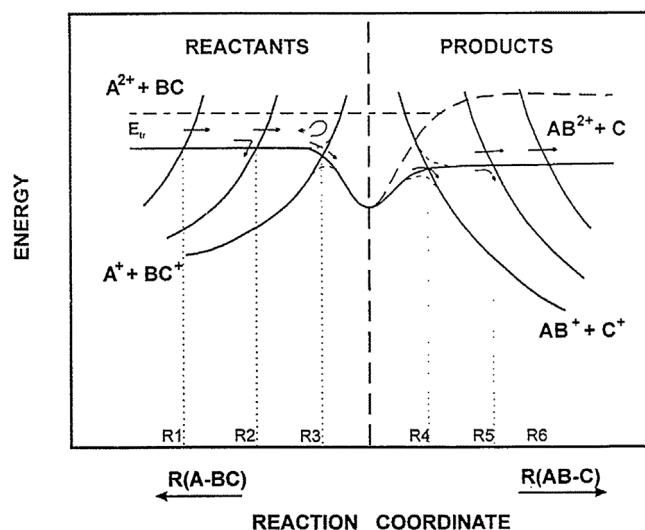
energy available in the reactions (exothermicity estimated at that time as 5.04 eV for Reaction (5) and 7.60 eV for Reaction (6)). The positions of the maxima in the $P(T')$ vs. T' plots for the electron transfer reaction (Fig. 6) were compared with maxima from of the $P(T')$ curves from collisions of CF_2^{2+} with Ar [35]; from the differences of the maxima, it could be concluded that about 1 or 2 vibrational quanta were most probably deposited as internal excitation of the other electron transfer product D_2^+. These experimental conclusions were supported by subsequent theoretical investigations of stationary points on the potential energy hypersurface [36].

On the basis of the available data, a simple potential model could be suggested which accounted for a competition of electron transfer and chemical reactions in the system molecular dication–neutral molecule [5,23,24]. A schematic of the model is given in Fig. 7: as the reactants ($A^{2+} + BC$) approach in the valley of the reactants on the dication surface, they meet with the Coulomb repulsive curves leading to the electron transfer products $A^+ + BC^+$ and may exit to these products, if the respective curve lies in some part of the reactions window, giving prevailingly or partly $A^+ + BC^+$. Only those reagent systems that did not end as electron transfer products continue further on the dication potential energy surface along the reaction coordinate and into the valley of the bond-forming products. There they cross with Coulomb repulsive curves leading to $AB^+ + C^+$ and may leave to end up as these chemical products. The model gives yet another possibility, namely, if the reactant systems end neither as electron transfer products $A^+ + BC^+$ nor chemical reaction products $AB^+ + C^+$, they may continue of the dication–neutral potential energy surface $A^{2+} + BC$ into the product valley and lead to dication–neutral bond-forming reactions $AB^{2+} + C$. The reactions of this type were observed earlier (see Reaction (4)) and recently in observation of the reactions like [37]

$$Ar^{2+} + N_2 \rightarrow ArN^{2+} + N \tag{7}$$

Formation of the ArN^{2+} in this collision system represented only a small, but important fraction of the dominant electron transfer.

The model was successfully applied in many cases including reactions of multiply-charged fullerenes with molecules [38] and, quite recently, to reactions of triply-charged ions with neutral molecules [39]. Also, it is in agreement with the occurrence of bond-forming reactions of aryl dications with small and larger
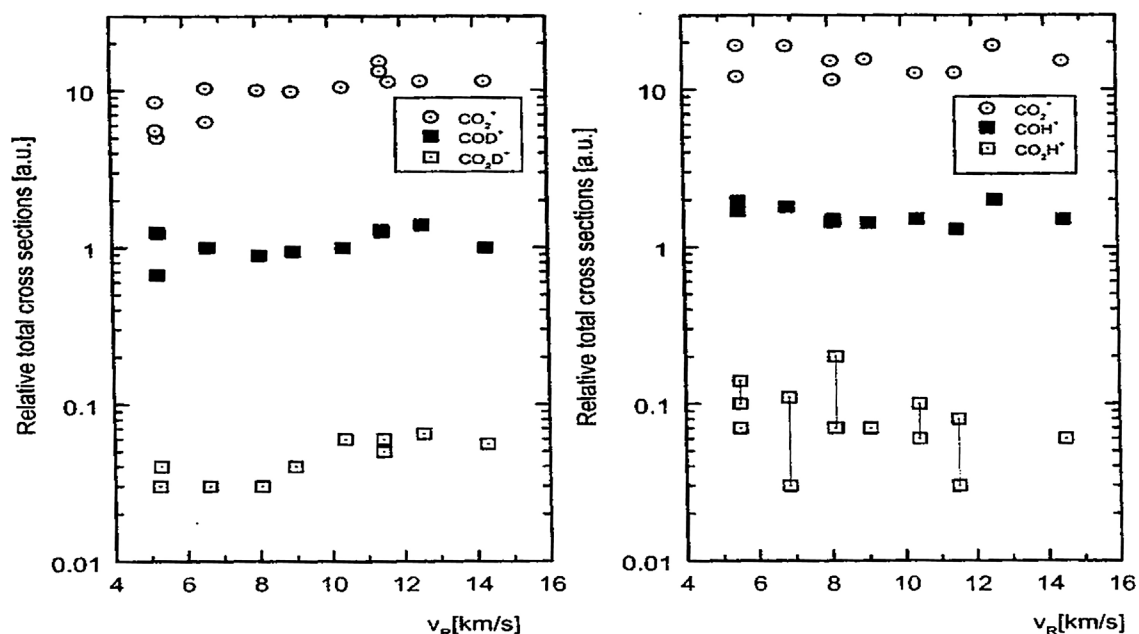
Fig. 8. Relative total cross sections for formation of products of reactions in the $CO_2^{2+} + D_2(H_2)$ system as a function of the relative velocity of the reagents, v_R.

molecules leading to dication products and carbon-chain building, as will be mentioned later on.

The model rationalizes relative probabilities of electron transfer and chemical reactions of dications depending on the mutual ratio of ionization energies of the species involved. If, for instance, the difference between the first and second ionization energy of the dication is smaller or comparable to the ionization energy of the neutral partner, the electron transfer is suppressed and there is a larger probability of bond-forming reactions, as in the case of earlier mentioned reactions of some metal dications with molecules [15,16].

3.1.2. $CO_2^{2+} + D_2$: Complex formation and subsequent dissociative processes

Relative total cross sections for the formation of products of collisions between CO_2^{2+} and D_2 [25] showed (Fig. 8) that the main process was non-dissociative electron transfer

$$CO_2^{2+} + D_2 \rightarrow CO_2^+ + D_2^+ \tag{8}$$

The cross section had little dependence on the relative velocity indicating that several states participate in the formation of the product, from the scattering data preferentially the $CO_2^+\left(A^2\Pi\right)$ and
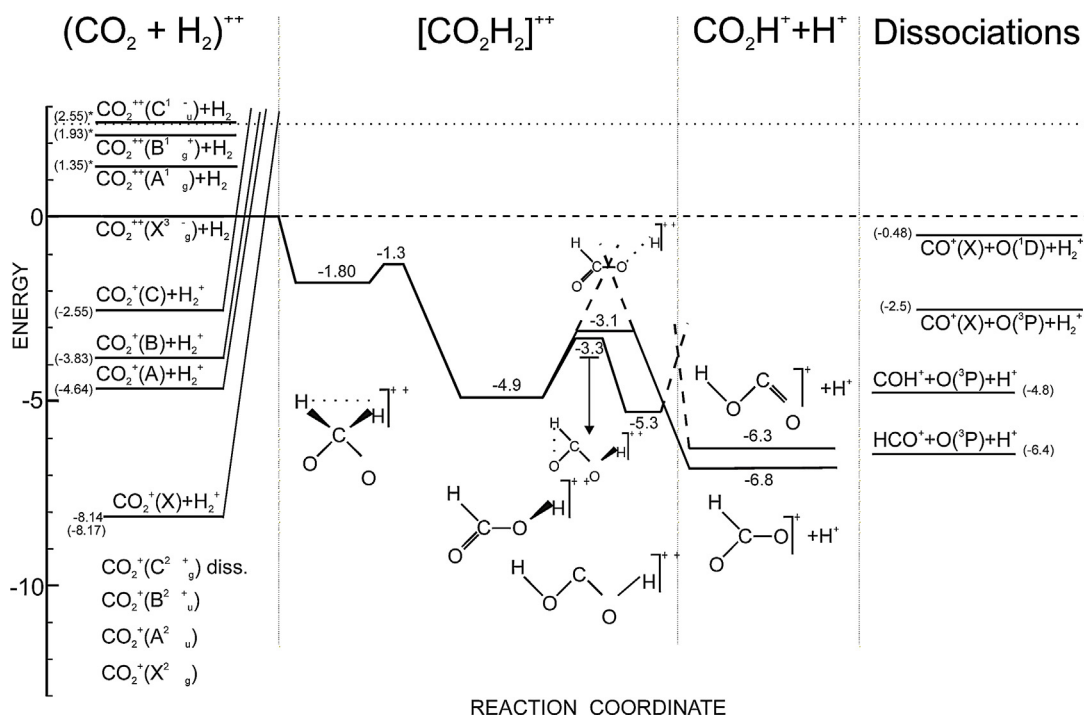

Fig. 9. Stationary points on the potential energy surface of $(CO_2H_2)^{2+}$. Numbers refer to the calculated values of energies of the species, intermediates, and transition states.
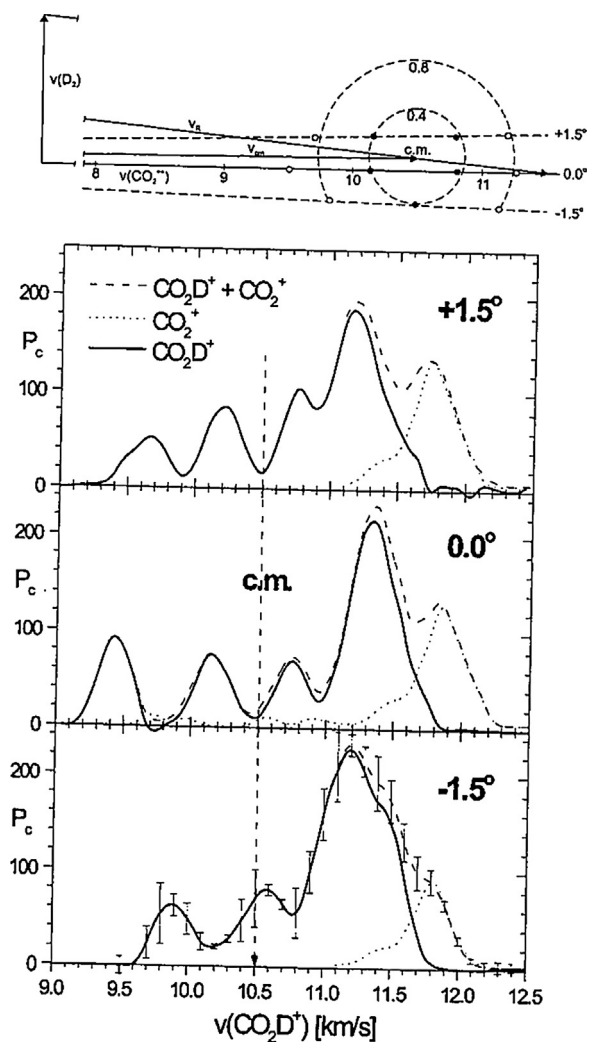
Fig. 10. Velocity profiles of CO_2D^+ from Reaction (9) at three different scattering angles, collision energy 2.5 eV. The section of the Newton diagram (upper part) shows the location of the maxima with respect to the CM of the system.

$CO_2^+\left(B^2\Sigma_u^+\right)$ states and a small amount was formed by the dissociation of the chemical reaction product CO_2D^+ [25].

The bond-forming reaction leading to CO_2D^+

$$CO_2^{2+} + D_2 \rightarrow CO_2D^+ + D^+ \tag{9}$$

represented only about 1% of the electron transfer reaction yield. On the other hand, the dissociative reaction giving COD^+ had a substantial cross section, about 10% of the electron transfer cross section. Stationary points on the potential energy surface of the system were calculated for the ground state of the $CO_2^{2+}\left(X^3\Sigma_g^-\right)$ (Fig. 9) and the calculations provided a justification of the experimental results: for electron transfer Reaction (8), population of $CO_2^+(A,B)$ of exothermicies 4.54 eV and 3.84 eV, respectively, fit the reaction window; deep well(s) on the way from reactants to bond-forming products justify the long-lived complex formation of different structures.

Scattering data of the bond-forming product of Reaction (9) are shown as velocity profiles measured along several scattering angles (Fig. 10). They showed two pairs of peaks symmetrically forward and backward with respect to the center-of-mass with the relative translational energy release of 0.45 eV and 4–4.5 eV, respectively. This indicated formation of the product CO_2D^+ by decomposition of intermediates $CO_2D_2^{2+}$. The inner peaks of about equal intensity suggested a long-lived intermediate of a mean

lifetime comparable to at least several average rotations of the complex $CO_2D_2^{2+}$, the outer peaks – uneven in height – a shorter-lived (osculating) complex of a mean lifetime comparable to about one average rotation of the complex. This finding was in agreement with the shape of the potential energy surface which exhibited rather deep minima on the way from reactants to the reaction products (Fig. 9). The channel of translational energy release of 4–4.5 eV was consistent with the formation of D—C-bonded isomer DCO_2^+ which dissociated further to $DCO^+ + O(HCO_2^+$ and $HCO^+ + O)$ in (Fig. 9).

The scattering diagrams for the dissociative product COD^+ (Fig. 11) was characterized by four peaks that could be understood as resulting from subsequent unimolecular decomposition of the higher-energy-release bond-forming product CO_2D^+ dissociating with an energy release COD^+–D of about 0.1–0.2 eV.

3.1.3. $CHCl^{2+} + D_2$: Facile proton transfer in chemical reactions of hydrogen-containing dications

The halogen-substituted dications of methylene CHX^{2+}, containing one hydrogen atom, were subjected to crossed-beam investigation of reactions with deuterium and rare gases. A study of reactions of $CHCl^{2+}$ showed that besides electron transfer leading to $CHCl^+$, two chemical reactions took place, namely [40]

$$CHCl^+ + D_2 \rightarrow CHDCl^+ + D^+ \tag{10}$$

and

$$CHCl^+ + D_2 \rightarrow CCl^+ + HD_2^+ \tag{11}$$

Detailed studies of electron transfer with rare gases [41] and adjoining theoretical studies [41,42] showed that two isomers of the dication of different energetics, with H bonded to the C atom ($HCCl^{2+}$) or to the Cl atom ($CClH^{2+}$), existed in the beam.

The scattering diagram of $CHDCl^+$ from Reaction (10) showed two pairs of peaks symmetrically located forward and backward with respect to the CM (Fig. 12). The inner pair of peaks, equal in intensity with the most probable translational energy release of about 1.1 eV implied a decomposition of a long-lived intermediate. The outer pair of peaks, uneven in intensity, with the most probable translational energy release of about 4.7 eV suggested a shorter-lived intermediate of an average lifetime of approximately one average rotation of the of a prolate complex, close to linear in its transition state. Theoretical calculations [42] showed several pathways involving both isomers of the dication and resulting in product cation of structures (H—C—Cl—H$^+$) and (H$_2$CCl$^+$). The collision resulted in both cases in a loosely-bound intermediate dication which dissociated directly to $CH_2Cl^+ + H^+$ and could be identified with the short-lived complex (outer peaks in Fig. 12). Alternately, the primary intermediate rearranged to the dication H_2CClH^{2+} and several pathways with rather deep minima were consistent with the decomposition of the long-lived intermediate [42].

The scattering diagram for CCl^+ from Reaction (11) exhibited (Fig. 13) a pair of peaks of about equal intensity symmetrically forward and backward from the center-of-mass. Analysis of the data and theoretical calculations led to the conclusion that this product resulted from further decomposition of vibrationally excited primary product of Reaction (10), $CHDCl^+$. However, the main feature in the diagram was a very strong forward peak, implying a direct mechanism of the reaction, with a high translational energy release of 5.6 eV, close to the exothermicity of Reaction (11), 5.3 eV. This strongly suggested a proton transfer Reaction (11) leading to CCl^+ and D_2H^+ as the other reaction product (this product scattered backward over a wide range of angles could be only barely identified among the reaction products). The facile proton transfer reaction from dications

containing hydrogen turned out to be a rather frequent reaction of these species with molecules.

Analogous conclusions could be drawn from experimental and theoretical studies of the reactions between $CHBr^{2+}$ and molecular hydrogen [43]. Two isomeric forms of the dication were identified, too, and the prominent chemical reaction was proton transfer and formation of $CBr^+ + H_3^+$. Theoretical calculations fully supported the experimental results obtained from beam scattering and deuterium labeling experiments. An important addition to the beam experiments came from comparison of the data on reactivity of CHX^{2+} dications ($X = F, Cl, Br, I$) with a series of atoms and simple non-polar and polar molecules [44]. Competition between electron transfer and bond-forming reactions showed that with atoms and non-polar molecules electron transfer was the dominant process, if its exothermicity fell into the reaction window. However, with polar molecules (CO, H_2O, HCl) proton transfer became much more important (from a few percent for non-polar neutrals to 20–60% for polar neutrals). The reason for it might be in the enhanced lifetime of collision complexes with polar neutral reagents [44].

Another system with hydrogen-containing dication studied by crossed-beam scattering and by tandem (quadrupole–octupole–quadrupole) mass spectrometric techniques was the interaction of the hydrocarbon dication $C_4H_3^{2+}$ with a series of atoms (Kr, Xe) and molecules (H_2, N_2, NO, NH_3, C_2H_2, CH_4) [45]. Both non-dissociative electron transfer reaction

$$C_4H_3^{2+} + M \rightarrow C_4H_3^+ + M^+ \tag{12}$$

and chemical reaction

$$C_4H_3^{2+} + M \rightarrow C_4H_2^+ + MH^+ \tag{13}$$

was observed. The results were complicated by the dissociative electron transfer reaction

$$C_4H_3^{2+} + M \rightarrow C_4H_2^+ + +H + M^+ \tag{14}$$

This required detailed analysis of the scattering diagrams and of the product relative translational energy distributions with the help of a new critical evaluation of the energetics of the dication $C_4H_3^{2+}$ and other hydrocarbon species involved. Chemical reaction (13) was found to be a strong-forward peaked direct process. Relative probabilities of reactions (12)–(14) showed the predominant role of electron transfer and dissociative electron transfer (Fig. 14), with the exception of the reaction with polar NH_3 (50% of bond-forming reaction (13)), in agreement with conclusions of [44].
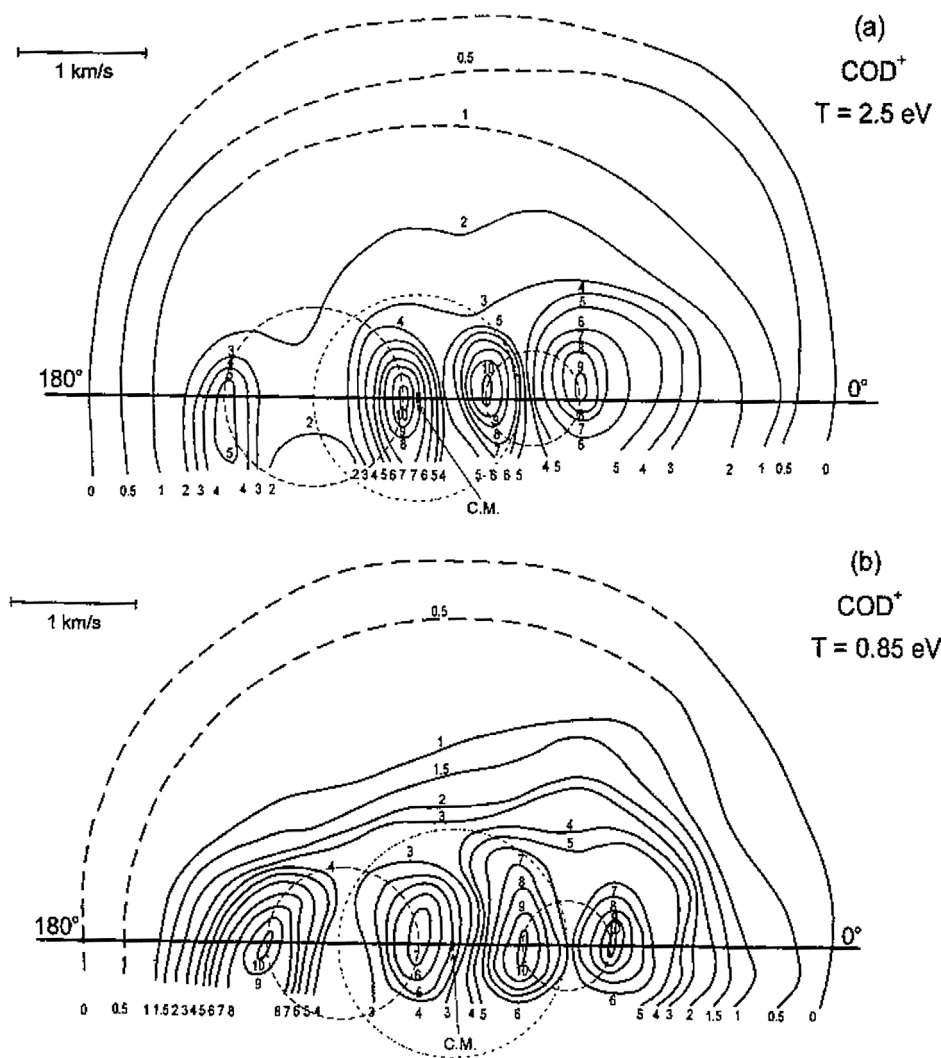

Fig. 11. Contour scattering diagram of COD^+ at two collision energies. The dash-dotted circle about the CM indicates the location of inner maxima of the CO_2D^+ velocity profiles (Fig. 10). The circles about the intersections of this circle with the direction of the relative velocity (horizontal line) indicate centers for the slow dissociative process leading to forward–backward wings of the COD^+ scattering.
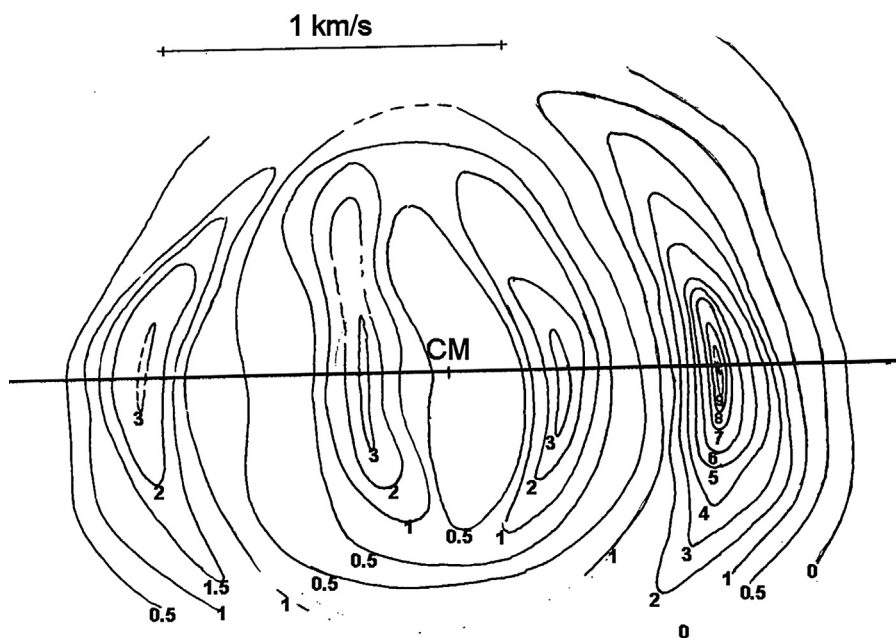
Fig. 12. Contour scattering diagram of CHDCl$^+$ from Reaction (10) at $T = 2.16$ eV. Designations analogous as in the previous scattering diagrams.

3.1.4. More complex reactions

A computational and experimental investigation of HCF$_2^+$ formation [46] in reaction

$$CF_3^{2+} + D_2 \rightarrow DCF_2^+ + (F + D)^+ \qquad (15)$$

resulted in "ab initio" quantum chemical calculations of the species involved and of the stationary points on the potential hypersurface of this system (Fig. 15). Two different pathways were identified leading to H$^+$ + F and HF$^+$ products. The crossed beam experiments revealed two distinct channels of DCF$_2^+$ formation with different translational energy release (Fig. 15). A comparison between reaction exothermicities and translational energy release for different combinations of products led to the final interpretation

of the reaction channel of CM velocity of 750 ms^{-1} (outer circle in Fig. 15), with the help of the theoretical results (proton-loss pathway 1, Fig. 15), as being predominantly due to the sequence

$$CF_3^{2+} + D_2 \rightarrow D_2CF_2^{2+} + F \rightarrow DCF_2^+ + D^+ + F \qquad (16)$$
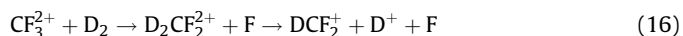
with the molecular product in its ground singlet state and translational energy release of about 7 eV (reaction exothermicity of 6.32 eV, collision energy 1.16 eV). Shallow wells associated with this pathway were consistent with the forward peaking of the product DCF$_2^+$ of this translational energy release. The channel of the CM velocity of 0.34 ms^{-1} indicated a process of intermediate complex formation and the interpretation was the same mechanism as previously (proton-loss pathway (1), however, with DCF$_2^+$
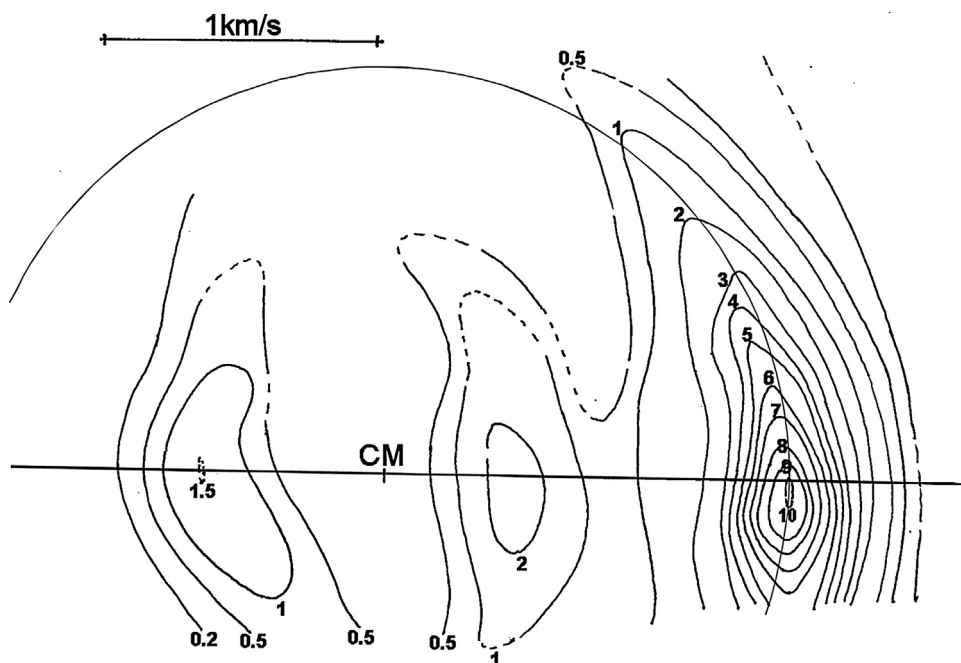

Fig. 13. Contour scattering diagram of CCl$^+$ at $T = 2.16$ eV. For explanation of the structures in it see text.
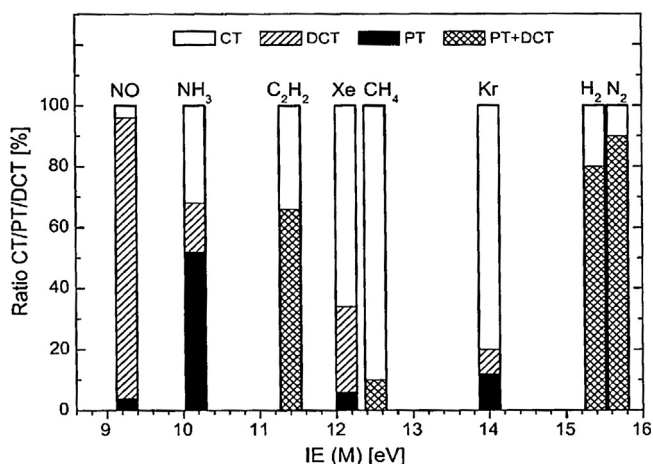
Fig. 14. Relative probabilities (in percent) of formation non-dissociative electron transfer (NDCT, open part of histograms), dissociative electron transfer DCT, (hatched), and proton transfer products (PT, black) as estimated from crossed-beam and mass spectrometric measurements in the dication–molecule system $C_4H_3^{2+}$ with the indicated molecules.

in its excited triplet state and of the translational energy release of about 1.5 eV (exothermicity of this channel 0.56 eV). The large upcoming part of the hypersurface toward DCF_2^+ in its triplet state forms a deep well on the way to the final product.
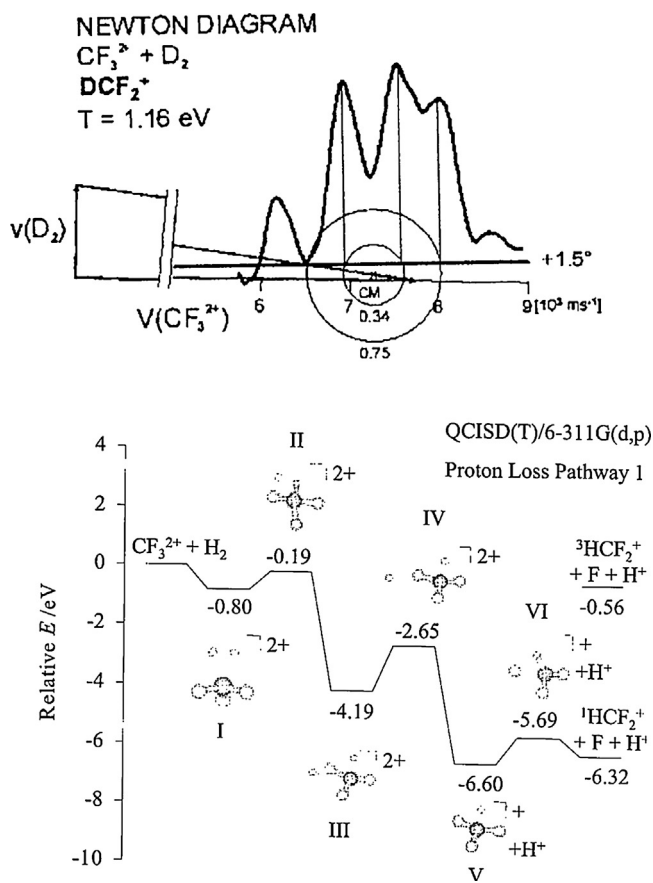

Fig. 15. A section of the Newton diagram with the velocity profile of DCF_2^+ from Reaction (15) at $T = 1.16$ eV. The circles indicate the product velocities relevant to the location of peaks in the distribution (upper part). Lower part: calculated stationary points on the proton-loss pathway I used in the explanation of the dynamics (see text).
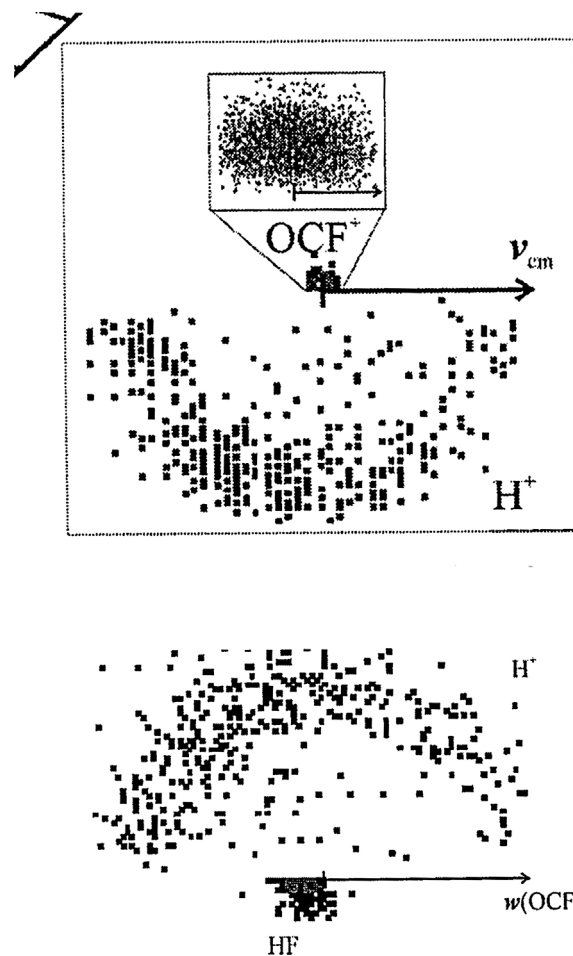

Fig. 16. Upper part: scattering diagram of products of Reaction (17) obtained by the PSCO technique and showing the motion of H^+ and OCF^+ (collision energy 5.6 eV). Inset shows expanded scattering of OCF^+. Lower part: internal frame scattering diagram showing the motion of H^+ and derived motion of neutral HF from Reaction (17) relative to OCF^+.

3.2. Coincidence experiments

Interpretation of dissociative electron transfer and bond-forming reactions leading to more than two products requires the assumption of subsequent decomposition of the primary reaction product out of the field of the departing primary products, if only one product ion is measured. The problems could be solved by registering more than one of the final products. The London
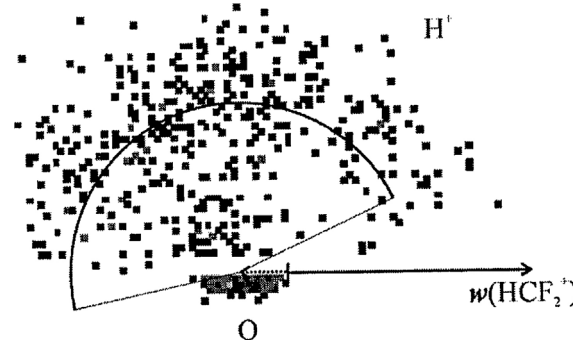

Fig. 17. Internal frame scattering diagram showing the motion of H^+ and derived motion of neutral O, formed in Reaction (18), relative to HCF_2^+.
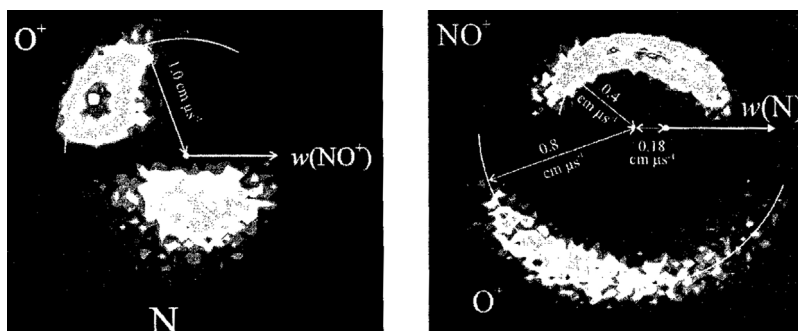
Fig. 18. Left: internal frame contour scattering diagram from PSCO experiments showing the motion of O^+ and N from Reaction (19) relative to NO^+ ($T = 7.1$ eV). Right: internal frame contour scattering diagram showing the motion of NO^+ and O^+ from the same reaction relative to the neutral N.

position sensitive coincidence (PSCO) apparatus described above provided an access to studies of reactions of this type.

3.2.1. $CF_2^{2+} + H_2O$: Different mechanisms of OCF^+ and HCF_2^+ formation.

One of the first bond-forming reactions studied by the PSCO technique was the reaction between CF_2^{2+} and H_2O [47]. Theoretical calculation of the stationary points on the potential energy hypersurface indicated an analogous shape of the surface as for the reaction $CO_2^+ + D_2$ (Fig. 9), implying formation of a long-lived complex. Experiments using PSCO revealed formation of bond-forming products OCF^+ and to a lesser extent HCF_2^+ in reactions

$$CF_2^{2+} + H_2O \rightarrow OCF^+ + H^+ + HF \qquad (17)$$

and

$$CF_2^{2+} + H_2O \rightarrow HCF_2^+ + H^+ + O \qquad (18)$$
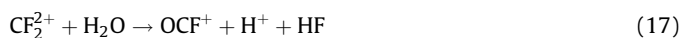
The scattering diagram of products of Reaction (17) is shown in Fig. 16. The scattering of H^+ was approximately isotropic with respect to the CM velocity of the dication, the product OCF^+ was also isotropically scattered but with a much lower CM velocity. This result indicated formation of a long-lived complex with a mean lifetime longer than several rotational periods of such species. The velocity distribution derived for the neutral product HF was also isotropic and sharply anticorrelated with that of OCF^+ (Fig. 16). These results could be interpreted only if the collision complex decomposed to form H^+ and $(HO-CF_2)^+$ and this ion subsequently dissociated to HF and OCF^+. A slight asymmetry in the scattering of H^+ scattering with respect to OCF^+ could be accounted for if the dissociation of $(HO-CF_2)^+$ occurred within the field of the departing H^+ [47].

The scattering diagram for Reaction (18) showed H^+ approximately isotropically scattered with a large velocity with respect to the initial dication velocity. In contrast, HCF_2^+ was forward scattered and O backward scattered. The scattering of H^+ implied again a long-lived complex formation, but the difference in scattering of both the ion HCF_2^+ and neutral O indicated a different mechanism that in Reaction (17). The forward scattering of HCF_2^+ with respect to the initial velocity of the dication was indicative of a direct reaction mechanism in which CF_2^{2+} flew by H_2O, picked up the hydride ion, leaving OH^+ as the other reaction product; the OH^+ then lived long enough to rotate significantly before decaying to $H^+ + O$, both these products would be then mutually isotropically distributed (Fig. 17). Reaction (18) thus proceeded as a direct reaction to form HCF_2^+ and OH^+ with OH^+ subsequently dissociating to H^+ and O.

### 3.2.2. Reactions of N_2^{2+}. Formation of the $(N_2O_2)^{2+}$ complex

Reactions of the dication N_2^{2+} with oxygen are of ionospheric importance. Besides electron transfer and dissociative electron transfer, formation of NO^+ was observed in chemical reactions [48].

Exothermicity of the respective processes leading to $NO^+ + O^+ + N$ can range, depending on the product electronic states, between 1–12 eV. The scattering diagrams [48] showed that all products were sideways scattered over a rather large range of scattering angles and indicated involvement of an intermediate complex $(N_2O_2)^{2+}$. The scattering in the internal frame revealed anti-correlation of velocities NO^+ vs. O^+ and the derived scattering of the neutral N indicated low correlation with velocities of both ion products (Fig. 18). The suggested mechanism compatible with these findings involved formation of an intermediate which lost initially a neutral species and then dissociated

$$N_2^{2+} + O_2 \rightarrow (N_2O_2)^{2+} \rightarrow NO_2^{2+} + N \rightarrow NO^+ + O^+ + N \qquad (19)$$
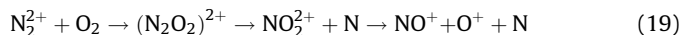
The mechanism was in agreement with energy considerations, involvement of electronic states of the species, theoretical calculations, and translational energy release as derived from the scattering diagrams. Theoretical considerations of the geometries of the $(N_2O_2)^{2+}$ complex suggested a tetrahedral stable structure and made it possible to estimate the mean lifetime of the complex to more than about 0.1 ps. Also, the structure pointed to a rotating complex dissociating from its critical configuration perpendicularly to its principal axis, in agreement with the sideways peaking of the products.

The scattering investigation of the analogous reaction leading to $NO^+ + N^+ + O$ [48] showed very similar results and led to the conclusion that Reaction (20) proceeded by a similar mechanism as Reaction (19), namely,

$$N_2^{2+} + O_2 \rightarrow (N_2O_2)^{2+} \rightarrow NO_2^{2+} + O \rightarrow NO^+ + N^+ + O \qquad (20)$$
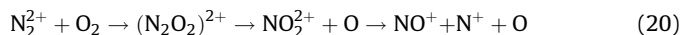
Scattering investigation of other reactions of the dication N_2^{2+} by the PSCO method revealed the dynamics of formation of ArN^+ in reaction of N_2^{2+} with Ar [28] and a series of bond-forming reactions in collisions with acetylene [28], water [28], and hydrogen [49].

In collisions of N_2^{2+} with hydrogen and deuterium the main reactions were non-dissociative and dissociative electron transfer. About 2% of the products resulted from bond-forming reaction leading to NH^+. Experiments using the PSCO method made it possible to reveal the correlations between the velocities of products and showed that NH^+ was formed by an N-atom loss from the intermediate complex $(N_2H_2)^{2+}$ to give the dication NH_2^{2+} which dissociated to $NH^+ + H$.

$$N_2^{2+} + H_2 \rightarrow (N_2H_2)^{2+} \rightarrow NH_2^{2+} + N \rightarrow NH^+ + H^+ + N \qquad (21)$$
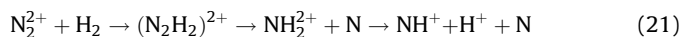
In interaction of Ar^{2+} with acetylene [50], the main reaction was dissociative single-electron transfer with a small contribution of dissociative double-electron transfer. The bond-forming reaction leading to ArC^+ represented about 1% of the products. Three different combinations of products could be identified $ArC^+ + CH^+ + H$; $ArC^+ + C^+ + H + H$; $ArC^+ + H^+ + C + H$. Studies by the coincidence technique revealed scattering very similar to the scattering
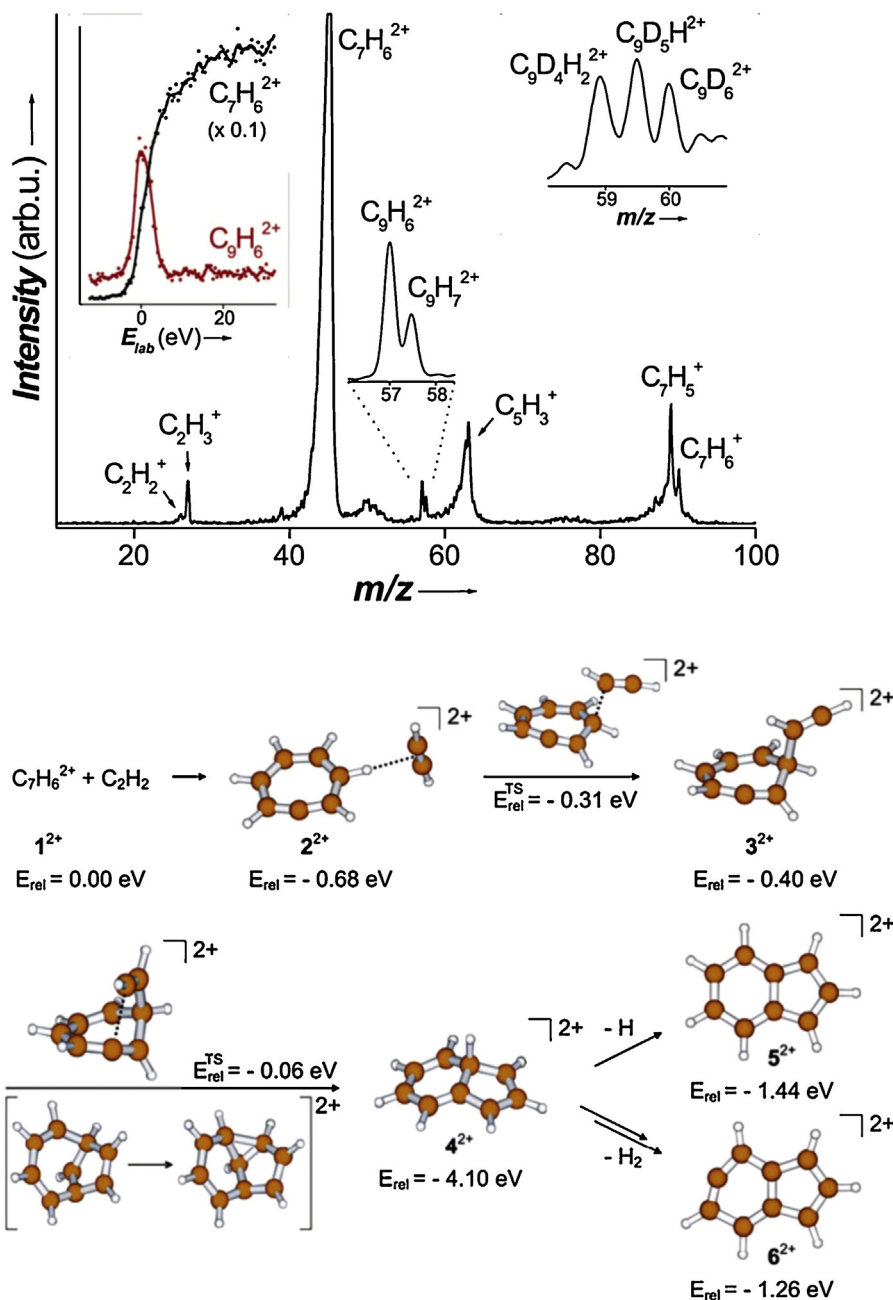
Fig. 19. Mass spectrometric data on Reaction (22) and (23) between $C_7H_6^{2+}$ and acetylene showing the relative intensities of the dication products $C_9H_7^{2+}$ and $C_9H_6^{2+}$. Left hand inset shows the same increase of the reagent $C_7H_6^{2+}$ and product $C_9H_6^{2+}$ signal with the collision energy, right-hand inset shows the H/D scrambling in $C_9H_nD_m^{2+}$ from $C_7D_6^{2+} - C_2H_2$ collisions.

of the single-electron transfer reactions. The product ion ArC$^+$ was scattered forward with respect to the center-of-mass in the direction of the incoming Ar^{2+} and the other ion product (H$^+$ or C$^+$ or CH$^+$) in the opposite direction. This implied an essentially direct mechanism of the reaction in which the dication stripped a CH$^-$ group from the neutral C_2H_2, formed ArCH^{+*} and CH$^+$; and the excited ArCH^{+*} subsequently dissociated.

3.3. Formation of polyaromatic dications in chemical reactions of dications

Numerous bimolecular chemical reactions of C_{60}^{2+} with simple molecules (H, water, unsaturated hydrocarbons, ammonia and amines) or a different organic molecules (alcohols, aldehydes,

ketones, esters, nitrogen heterocycles etc.) were reported from selected-ion-flow-tube (SIFT) studies of the C_{60}^{n+} reactivity [38]. In those the neutral partner M was fully attached to the C_{60} structure forming a $C_{60}M^{2+}$ dication product or led to a protonated cation product (reactions with RH). Electron transfer was in many cases an effective competing process.

A class of bond-forming reaction of doubly-charged arenes with neutral hydrocarbons leading doubly-charged hydrocarbon ions of a longer chain-length was observed in mass spectrometric experiments. Though the reactions were not investigated by the scattering methods (the studies would be difficult anyway, because of small recoil of heavy dications products on the light neutral product, H or H$_2$), they should be mentioned here, because of their general importance.

Besides non-dissociative and dissociative electron transfer reaction and chemical reactions in which two singly-charged products were formed, chemical reactions leading to doubly-charged products were observed and described [51] in studies of reactivity of doubly-charged ions from toluene with acetylene. Dication products of a longer carbon chain than the reactants were observed in reactions

$$C_7H_6^{2+} + C_2H_2 \rightarrow C_9H_7^{2+} + H \tag{22}$$

$$C_7H_6^{2+} + C_2H_2 \rightarrow C_9H_6^{2+} + H_2 \tag{23}$$
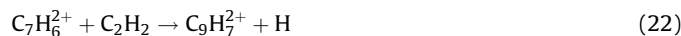
The participation of the doubly charged ion $C_7H_6^{2+}$ as a reactant in the reaction was confirmed by measuring the same energy dependence for it (Fig. 19) and the product $C_9H_6^{2+}$ and by deuterium labeling which also showed H/D scrambling in the product $C_9H_6^{2+}$ (Fig. 19) thus pointing to the formation of a long-lived complex in its formation. Theoretical studies [51] revealed the pathway for formation of the products in Reactions (22) and (23) (Fig. 19) and involvement of the indene skeleton in the sequence of structures leading to them.

Subsequent studies of reactions between different dications of the type $C_mH_n^{2+}$ (dications from benzene, indene, naphthalene, phenanthrene) and acetylene, benzene [51–53], and methane [54] showed that C—C bond-forming reactions of the above mentioned type are rather general and of possible importance for astrophysics as a route to polyaromatic hydrocarbons (PAH) in planetary atmosphere and interstellar media [52].

More recently, bond-forming reactions of dications from cycloheptatriene ($C_7H_6^{2+}$, $C_7H_8^{2+}$) with Xe and N_2 were described leading to products $C_7H_6Xe^{2+} + H_2$ and to adducts $C_7H_6Xe^{2+} + C_7H_6N_2^{2+}$ [55].

3.4. Reactions of molecular trications

Similarly as with C_{60}^{2+} dications, a series of chemical reactions of the trication C_{60}^{3+} was observed in SIFT experiments [38] with simple molecules or different organic molecules. The reactions led to addition of the neutral partner M to the trication and formation of trication products $C_{60}M^{3+}$ or to the dication product $C_{60}H^{2+}$ and a singly-charged fragment (OH+, R+ in reactions with H_2O and RH).

Very recently, reactions of the triply-charged ion I^{3+} with a series of neutral molecules, studied by time-of-flight technique, have been reported [56]. The charged product ions involve IO^{2+} (reactions with CO, CO_2, SO_2); IO+ (with CO_2, SO_2); IC^{2+} (with CO); IC+ (CS_2); IX^{2+} and IX+ (X = Cl in CH_3Cl, X = F in CHF_3); IN^{2+} and IN+ (with N_2O), and IS+ (with SO_2 and CS_2). The bond-forming products were formed in surprisingly large yields ranging from a few percent up to 50% of the product ion sum. Also, interactions between Xe^{3+} and CF_4 leading to bond-forming products XeF_2^{2+} and XeF+, and interactions between CS_2^{3+} and CF_3I leading to SF+ were observed.

In reactions with I^{3+} non-dissociative and dissociative electron transfer predominated, but chemical reactions represent a non-negligible part. A rationalization of the product formation and of their yields was carried out using the potential surface model [24] modified to involve triply-charged ions. Theoretical calculations of the stationary points on the hypersurface I^{3+}–CO indicated involvement of long-lived complexes in chemical product formation. Detailed scattering data using the PSCO techniques have been so far hampered by a low ion yield of triply-charged reagents.

4. Conclusions

The results of beam scattering experiments discussed in this contribution helped in understanding the dynamics of chemical (bond-forming) reactions of dications:

a) The distinction and competition between electron transfer and bond-forming reactions leading either to two Coulomb-repulsing chemical products or to dication–neutral chemical products was established and a potential energy model was developed which accounts correctly for competition of these reactions.

b) Described mechanisms of dication–neutral chemical reactions involve both direct reactions and intermediate complex formation and decomposition.

c) Dissociative processes turn out to be usually sequential unimolecular decompositions of the primary chemical product as concluded from crossed-beam experiments and confirmed by the position-sensitive coincidence experiments. However, the later method described some processes in which the dissociation took place still within the field of separating primary chemical products.

d) Theoretical calculations of stationary points on the potential hypersurfaces of the studied systems were of great importance in interpreting the experimental results, providing a significant help in elucidating the dynamics of the systems studied.

e) Recently described chemical reactions of triply-charged ions with molecules open a way to studying yet another class of multiply-charged–neutral reactions.

References

[1] D. Mathur, Phys. Rev. 391 (1996) 299.
[2] D. Schröder, H. Schwarz, J. Phys. Chem. A 103 (1999) 7385.
[3] S.G. Cox, A.D.J. Critchley, P.S. Kreynin, I.R. Nab, R.C. Shiel, F.E. Smith, Phys. Chem. Chem. Phys 5 (2003) 131.
[4] R.B. Metz, Int. J. Mass Spectrom. 235 (2004) 131.
[5] Z. Herman, Int. Rev. Phys. Chem. 15 (1996) 299.
[6] Z. Herman, Phys. Essays 13 (2000) 480.
[7] S.D. Price, Int. J. Mass Spectrom. 260 (2007) 1.
[8] Z. Herman, Mol. Phys. 111 (2013) 1697.
[9] R.K. Janev, H.-P. Winter, Phys. Rep. 117 (1985) 965.
[10] D. Mathur, Phys. Rep. 225 (1993) 193.
[11] J.J. Thomson, Rays of Positive Electricity, Cambridge University Press, Cambridge, 1921, pp. p. 84.
[12] K.G. Spears, F.C. Fehsenfeld, F. McFarland, E.E. Ferguson, J. Chem. Phys. 56 (1972) 2562.
[13] B.K. Chatterjee, R. Johnsen, J. Chem. Phys. 91 (1989) 1378.
[14] R. Tonkyn, J.C. Weisshaar, J. Am. Chem. Soc. 108 (1986) 7128.
[15] J.C. Weisshaar, Acc. Chem. Res. 26 (1993) 213.
[16] L.M. Roth, B.S. Freiser, Mass Spectrom. Rev. 10 (1991) 303.
[17] J.R. Gord, B.S. Freiser, S.W. Bruckner, J. Chem. Phys. 91 (1989) 7530.
[18] Y.A. Ranasighe, T.J. MacMahon, B.S. Freiser, J. Phys. Chem. 95 (1991) 7721.
[19] L.G. Parke, C.S. Hinton, P.B. Armentrout, J. Phys. Chem. A 112 (2008) 10469.
[20] S.D. Price, M. Manning, S.R. Leone, J. Am. Chem. Soc. 116 (1994) 8673.
[21] P.B. Armentrout, The Encyclopedia of Mass Spectrometry, in: M.L. Gross, R. Caprioli, (eds.), vol. 1 (P.B. Armentrout, Volume Ed.), Elsevier, 751–776, ISBN 0–08-043802–4.
[22] S.A. McLuckey, The Encyclopedia of Mass Spectrometry, in: M.L. Gross, R. Caprioli, (eds.), vol. 1 (P.B. Armentrout, Volume Ed.), Elsevier, 866–877, ISBN 0–08-043802–4.
[23] Z. Dolejšek, M. Fárník, Z. Herman, Chem. Phys. Lett. 235 (1995) 99.
[24] Z. Herman, J. Žabka, Z. Dolejšek, M. Fárník, Int. J. Mass Spectrom. 192 (1999) 191.
[25] L. Mrázek, J. Žabka, Z. Dolejšek, J. Hrušák, Z. Herman, J. Phys. Chem. A 104 (2000) 7247.
[26] Z. Herman, Int. J. Mass Spectrom. 212 (2001) 413.
[27] S.D. Price, Phys. Chem. Chem. Phys. 5 (2003) 1717.
[28] W.P. Hu, S.M. Harper, S.D. Price, Meas. Sci. Technol. 13 (2002) 1512.
[29] S.D. Price, Int. J. Mass Spectrom. 260 (2007) 1.
[30] N. Tafadar, N. Kaltsoyannis, S.D. Price, Int. J. Mass Spectrom. 192 (1999) 205.

[31] J. Roithová, D. Schröder, P. Grüne, T. Weiske, H. Schwarz, J. Phys. Chem. A 110 (2006) 2970.
[32] J. Roithová, D. Schröder, Phys. Chem. Chem. Phys. 9 (2007) 731.
[33] D. Bassi, P. Tosi, R. Schlögl, J. Vac. Sci. Technol. A 16 (1998) 114.
[34] B. Friedrich, Z. Herman, Chem. Phys. Lett. 107 (1984) 375.
[35] J. Žabka, Z. Herman, Czech J. Phys. 49 (1999) 373.
[36] N. Tafadar, S.D. Price, Int. J. Mass Spectrom. 223-224 (2003) 547.
[37] P. Tosi, R. Correale, W. Lu, S. Falcinelli, D. Basi, Phys. Rev. Lett. 82 (1999) 450.
[38] D.K. Bohme, Mass Spectrom. Rev. 28 (2009) 672.
[39] J.D. Fletcher, M.A. Parkes, S.D. Price, Chem. Eur. J. 19 (2013) 10965.
[40] J. Roithová, J. Žabka, J. Hrušák, R. Thissen, Z. Herman, J. Phys. Chem. A 107 (2003) 7347.
[41] J. Roithová, J. Žabka, R. Thissen, Z. Herman, Phys. Chem. Chem. Phys. 5 (2003) 2988.
[42] J. Roithová, J. Hrušák, Z. Herman, J. Phys. Chem. A 107 (2003) 7355.
[43] J. Roithová, J. Žabka, Z. Herman, R. Thissen, D. Schröder, H. Schwarz, J. Phys. Chem. A 110 (2006) 6447.
[44] J. Roithová, Z. Herman, D. Schröder, H. Schwarz, Chem. Eur. J. 12 (2006) 2465.
[45] J. Jašík, J. Roithová, J. Žabka, R. Thissen, I. Ipolyi, Z. Herman, Int. J. Mass Spectrom. 255–256 (2006) 150.
[46] N. Lambert, N. Kaltsoyannis, S.D. Price, J. Žabka, Z. Herman, J. Phys. Chem. A 110 (2006) 2898.
[47] S.M. Harper, S.W.P. Hu, S.D. Price, J. Chem. Phys. 121 (2004) 3507.
[48] C.L. Ricketts, S.M. Harper, S.W.P. Hu, S.D. Price, J. Chem. Phys. (2005) 123 (Art. no. 134,422).
[49] J.F. Lockyear, C.L. Ricketts, M.A. Parkes, S.D. Price, Chem. Sci. 2 (2011) 150.
[50] M.A. Parkes, J.F. Lockyear, S.D. Price, Int. J. Mass Spectrom. 280 (2009) 85.
[51] J. Roithová, D. Schröder, J. Amer. Chem. Soc. 128 (2006) 4208.
[52] J. Roithová, D. Schröder, Phys. Chem. Chem. Phys. 9 (2007) 2341.
[53] J. Roithová, D. Schröder, Phys. Chem. Chem. Phys. 9 (2007) 731.
[54] J. Roithová, C.L. Ricketts, D. Schröder, Int. J. Mass Spectrom. 280 (2009) 32.
[55] D. Ascenzi, J. Aysina, E.-L. Zins, D. Schröder, J. Žabka, C. Alcaraz, S.D. Price, J. Roithová, Phys. Chem. Chem. Phys 13 (2011) 18330.
[56] J.D. Fletcher, M.A. Parkes, S.D. Price, Chem. Eur. J. 19 (2011) 10965.